Applied Science, Computing and Energy, 2026, 4(4), 198-216

Application of Multi-fractal Modeling and Multivariate Statistical Analysis to Stream Sediment Data for Assessing the Mineralization Potential in the Akpet area, Southeastern Nigeria

Benjamin Odey Omang*, Godwin Terwase Kave, Enah Asinya Asinya, Temple Okah Arikpo, Idris Nurudeen Gimba, and Anthony Adesoji Onasanwo
17 September 2025/Accepted: 12 March 2026 /Published: 30 March 2026

Abstract: *The search for new mineral resources in southeastern Nigeria is necessary for supporting industrial growth and advancing sustainable resource development. The Akpet area is a prospective area for economic mineral exploration. This study applies multivariate statistical analysis and multifractal modeling to stream sediment geochemistry in the Akpet area, southeastern Nigeria, with the aim of assessing its mineralization potential. A total of fifteen (15) stream sediment samples were systematically collected from active stream and river channels and analyzed using inductively coupled plasma–mass spectrometry (ICP-MS). Geochemical results revealed enrichment of elements such as Cr, Cs, Rb, Zr, Hf, Th, and U relative to upper continental crust (UCC). In contrast, Co, Cu, Ni, Pb, Zn, V, Sc, and Sr were depleted. Pearson correlation and principal component analysis (PCA) reveals association of U–Th–Zr–Mo, reflecting possible radioactive mineralization. Complementary multifractal concentration–number (C–N) modeling distinguished three geochemical populations; low background, high background, and weakly anomalous for Ba, Cu, Mo, Ni, Pb, Th, U, and Zn. Anomalous thresholds were highest for Mo, U, and Th, reflecting possible radioactive mineralization in the study area.*

Keywords: *Geochemistry, fractal modeling, Statistics, Mineralization, Akpet, Southeastern Nigeria.*

Benjamin Odey Omang
Department of Geology, University of Calabar, P.M.B 1115, Calabar, Cross River State, Nigeria
Email: odeyben@gmail.com
https://orcid.org/0000-0001-9196-3109

Godwin Terwase Kave
Department of Geology, University of Calabar, P.M.B 1115, Calabar, Cross River State, Nigeria
Email: gkaves@yahoo.com

Enah Asinya Asinya
Department of Geology, University of Calabar, P.M.B 1115, Calabar, Cross River State, Nigeria
Email: asinyaenya@gmail.com

Temple Okah Arikpo
Department of Geology, University of Calabar, P.M.B 1115, Calabar, Cross River State, Nigeria
Email: arikpotemple@gmail.com
***h*ttps://orcid.org/0009-0002-9425-0125**

Idris Nurudeen Gimba
Department of Geology, University of Calabar, P.M.B 1115, Calabar, Cross River State, Nigeria
Email: updeen177@yahoo.com

Anthony Adesoji Onasanwo
Department of Geology, University of Calabar, P.M.B 1115, Calabar, Cross River State, Nigeria
Email: adsojt@gmail.com

1.0 Introduction

Nigeria is a country that is richly endowed with a wide variety of mineral resources, many of which are hosted in its Precambrian basement rocks and younger sedimentary basins. Over the years, the demand for solid minerals such as gold, tantalite, columbite, beryl, copper, vanadium, and lithium, has grown because of their industrial and economic importance (Oyawoye, 1964; Obaje, 2009). Southeastern Nigeria, where the Akpet area is located, lies within the Basement Complex terrain that has undergone several geological processes including magmatism, metamorphism, and deformation. These processes often create favorable conditions for mineralization (Yohe, 2024).

Stream sediments are one of the most useful sampling media in mineral exploration. As water flows across different rocks and soils, it carries fine particles downstream. These particles preserve geochemical signatures of the rocks they are derived from. By analyzing stream sediments, it is possible to detect abnormal

concentrations (anomalies) of certain elements that may indicate the presence of mineral deposits upstream (Garba, 2003).

To derive meaningful insights out of large geochemical datasets, the use of multivariate statistical methods such as correlation analysis, cluster analysis, and principal component analysis (PCA) is widely utilized. These methods help to identify groups of elements that occur together, which may reflect a common source or mineralizing process. For example, associations of gold (Au) with arsenic (As) and antimony (Sb) are well-known indicators of gold mineralization (Adekoya, 2003). Such statistical tools reduce data complexity and highlight the most important geochemical patterns related to mineralization (Esmaeili *et al*., 2014).

However, statistical methods alone sometimes struggle to capture the irregular and complex distribution of geochemical anomalies. This is where multifractal modeling becomes important. Multifractal analysis is based on fractal mathematics and is used to describe patterns that vary across multiple scales. In geochemical exploration, multifractal models such as the concentration–area (C–A) and concentration–number (C–N) methods are applied to separate background geochemical values from weak and strong anomalies. This provides a more objective and precise way of defining geochemical thresholds (Cheng *et al*., 1994).

In recent years, the integration of multivariate statistics and multifractal modeling has gained more attention in geochemical exploration. While multivariate analysis identifies relationships among elements, multifractal modeling distinguishes anomalies from natural background variations more effectively (Afzal *et al*., 2010). This combined approach improves the accuracy of accessing mineralization potential in a particular area.

The Akpet area in southeastern Nigeria is geologically significant because it is underlain by basement rocks that are known to host pegmatites. Despite this potential, limited research has applied advanced techniques such as multifractal modeling to model the geochemical dataset with this region. Most previous works in southeastern Nigeria have focused on traditional geologic mapping and basic geochemical interpretation, leaving a gap in the application of integrated statistical and multifractal methods (Olade, 2021; Garba, 2003).

Therefore, this study seeks to apply multivariate statistical analysis and multifractal modeling to stream sediment geochemical data from the Akpet area. The goal is to identify elemental associations, delineate geochemical anomalies, and assess the mineralization potential of the study area. This research will not only contribute to understanding the resource geology of Akpet but also provide a framework for more efficient mineral exploration in other parts of Nigeria.

1.1 The Study Area

The Akpet area is located in the southeastern part of Nigeria, within Cross River State. Geographically, it lies between latitudes 5°30′N and 6°00′N and longitudes 8°00′E and 8°30′E. The study area is part of the Oban Massif terrain with granodiorite as the predominant lithology (Figure 1), which forms a rugged basement complex terrain with elevations ranging from lowlands in river valleys to moderately high hills (Ekwueme, 2003; Omang *et al*., 2024). The topography is generally undulating, with ridges and valleys that control the flow of streams and rivers. Drainage is mainly dendritic, meaning that the streams branch out in a tree-like pattern, which is typical of crystalline basement terrains. Major rivers and streams in the area include tributaries of the Cross River, which serve as important sites for stream sediment accumulation and transport of mineral particles. The Akpet area lies within the tropical rainforest belt of southeastern Nigeria. The climate is typically hot and humid, with a distinct wet season (April to October) and dry season (November to March). Annual rainfall ranges between 2,000–3,000 mm, with heavy rains that encourage weathering of rocks and transport of sediments by surface water. Vegetation is dominated by thick forests, and farmlands. These provide both natural cover and human-modified landscapes that influence soil erosion and sedimentation.

2.0 Materials and Method

A total of fifteen (15) stream sediment samples were systematically collected from active stream and river channels within the Akpet area. The sampling points were strategically selected to ensure adequate spatial coverage and to target

locations with active sediment deposition, as recommended for geochemical exploration studies (Govett, 1983; Salminen *et al*., 2005; Omang *et al*.,2026). Stream sediments were chosen because they represent an integrated geochemical signal of the upstream drainage basin, thereby serving as an effective medium for identifying potential mineralization anomalies (Rose, Hawkes, & Webb, 1962). At each site, sediments were collected from the upper 5–10 cm of the active channel bed using a pre-cleaned plastic scoop to minimize contamination, following standard geochemical sampling protocols (Smith *et al*., 2005).

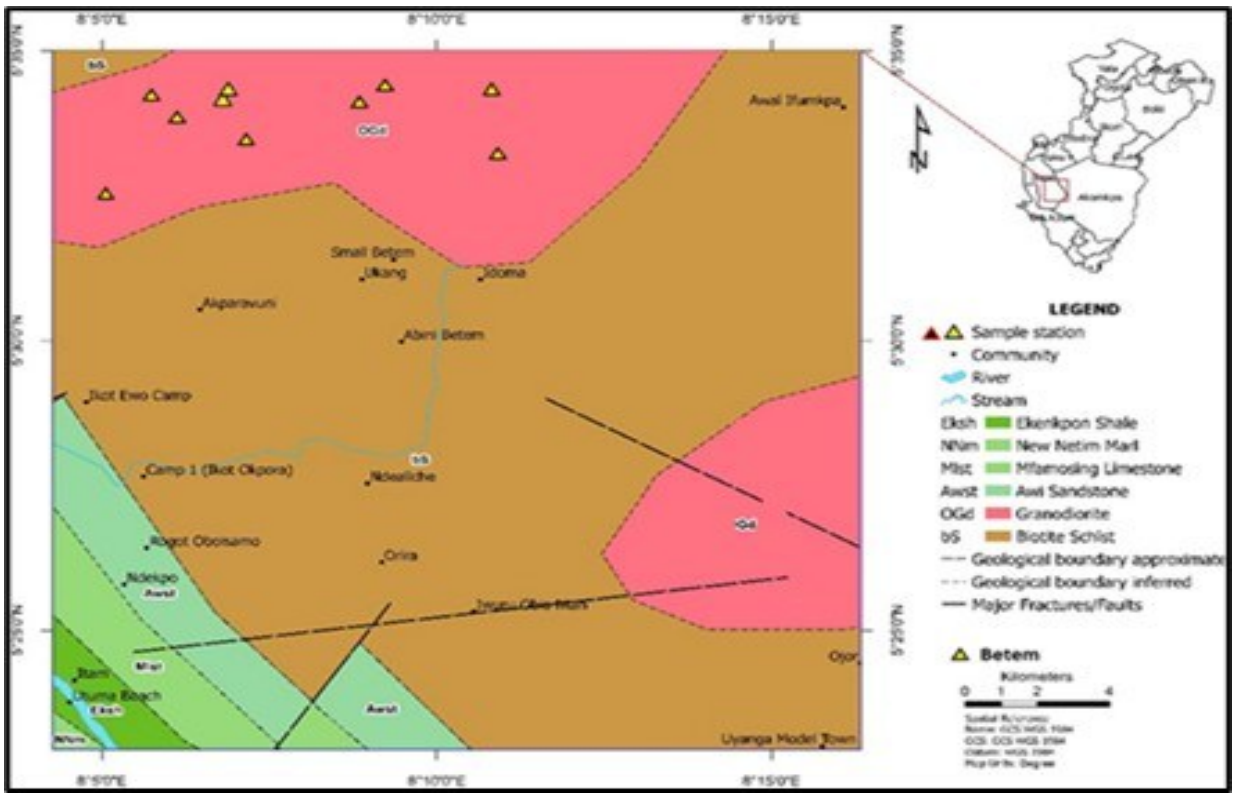

Fig. 1. Geology map of the study area

Coarse gravel and organic debris were removed on site, and the fine fraction (<2 mm) was retained, as this size fraction has been shown to best reflect the geochemical composition of the source rocks (Govett, 2013). Each sample was placed in a sealed, labeled polyethylene bag and recorded with its corresponding GPS coordinates using a handheld GPS device (±3 m accuracy). The collected stream sediment samples were air-dried at ambient temperature to prevent loss of volatile components and to maintain sample integrity (Griffiths, 1967). Once dried, the samples were gently disaggregated using a porcelain mortar and pestle to avoid metal contamination, following established sample preparation protocols (Govett, 1983; Reimann & Filzmoser, 2000). The disaggregated material was sieved through a 75 µm stainless steel mesh to isolate the fine fraction, which is widely recognized as the most geochemically homogeneous and representative for detecting mineralization anomalies due to its large surface area and higher metal adsorption capacity (Salminen *et al*., 2006).

Prepared samples were shipped to Activation Laboratories (ACTLABS), Ontario, Canada, for trace element analysis. The analytical procedure employed was Inductively Coupled Plasma Mass Spectrometry (ICP–MS).

Prior to statistical analysis, the raw geochemical data were examined for compositional effects inherent in closed datasets. Geochemical datasets derived from stream sediment analysis are compositional in nature, meaning that the concentrations of all measured elements sum to a constant, which can induce spurious correlations and distort multivariate statistical

results if not addressed (Aitchison, 1982; Reimann *et al*., 2002).

To mitigate this closure effect, a centered log-ratio (clr) transformation was applied to the data. The clr transformation expresses each component relative to the geometric mean of all components in the sample, thus allowing for subsequent statistical treatments to be carried out in an unconstrained Euclidean space (Filzmoser *et al*., 2009). The transformation was performed using the equation:

$$clr(x_i) = \ln\left(\frac{x_i}{g(x)}\right) \quad (1)$$

where x_i is the concentration of the i-th element, and g(x) is the geometric mean of all elements in the samples. Before transformation, values below detection limits were replaced with one-half of the detection limit for the respective element to avoid mathematical inconsistencies when applying logarithmic functions (Helsel, 2011). The clr-transformed dataset was then used for all subsequent multivariate statistical analyses to ensure valid interpretation of geochemical relationships and anomaly patterns.

3.0 Results and Discussion

3.1. Trace element geochemistry

The results of the trace element geochemistry of stream sediment samples from the Akpet area are presented in Table 1 and 2. Concentrations of the analyzed elements show moderate variability, with values generally falling within ranges typical of upper continental crust (UCC) compositions (Taylor & McLennan, 1985; Rudnick, 2005).

Barium (Ba) concentrations range from 350.86 to 373.47 ppm, with a mean of 362.22 ppm. These values are slightly lower than the average UCC concentration of 550 ppm (Rudnick, 2005). Cobalt (Co) varies between 3.82 and 4.20 ppm (mean = 4.01 ppm), which is significantly below the UCC average of approximately 17 ppm (Taylor & McLennan, 1985). Chromium (Cr) displays relatively high concentrations, ranging from 419.69 to 489.92 ppm (mean = 473.65 ppm). These values exceed the UCC reference value of approximately 92 ppm (Rudnick & Gao, 2003). Cesium (Cs) values (1.88–2.10 ppm; mean = 2.00 ppm) are slightly higher than the UCC average of 1.5 ppm, whereas rubidium (Rb) concentrations (130–210 ppm; mean = 173.21 ppm) are markedly enriched compared to the UCC value of approximately 84 ppm.

Copper (Cu) concentrations are relatively low (12.36–13.61 ppm; mean = 12.87 ppm), slightly below the UCC average of 25 ppm. Similarly, nickel (Ni) shows concentrations between 15.61 and 17.84 ppm (mean = 17.05 ppm), which are considerably lower than the UCC value of approximately 47 ppm (Rudnick, 2005). Lead (Pb) varies between 11.86 and 12.47 ppm (mean = 12.20 ppm), which is slightly below the UCC concentration of 17 ppm. Zinc (Zn) shows values between 14.47 and 15.75 ppm (mean = 15.13 ppm), far below the UCC average of 67 ppm. High field strength elements (HFSEs) including Zr, Hf, Th, and U are moderately enriched. Zirconium (Zr) concentrations range between 230.95 and 261.88 ppm (mean = 250.45 ppm), close to the UCC average of 190 ppm. Hafnium (Hf) (5.83–6.39 ppm; mean = 6.09 ppm) and thorium (Th) (13.20–14.74 ppm; mean = 14.15 ppm) are also slightly higher than UCC averages (Hf ~5 ppm; Th ~10 ppm). Uranium (U), however, shows values (1.35–1.47 ppm; mean = 1.41 ppm) similar to UCC averages (~2.7 ppm). Transition metals such as vanadium (V) and scandium (Sc) occur at relatively low levels, with V ranging from 15.45 to 16.70 ppm (mean = 16.00 ppm) compared to UCC average of 97 ppm, and Sc ranging from 2.01 to 2.18 ppm (mean = 2.09 ppm) with UCC average of 14 ppm. Yttrium (Y) shows concentrations (9.51–10.48 ppm; mean = 9.94 ppm), slightly lower than the UCC average of 22 ppm. Strontium (Sr) values range from 48.08 to 59.04 ppm (mean = 56.15 ppm), much lower than the UCC average of 320 ppm. The mean concentrations of all the analyzed element are below the calculated threshold values.

4.2 Fractal/multifractal modeling

The Concentration number (C-N) plot of Ba produced three statistical populations (as seen in Figure 2). The first statistical population ranges from 350.86 ppm to 354.89ppm, indicating low background. The second population ranges from 358.14ppm to 368.75ppm, reflecting high background concentration. The third population, ranges from 368.82ppm to 373.47ppm, indicating a weak anomaly. The C-N fractal analysis of Cu reveals three statistical populations (Figure 3).

Table 1: Concentrations of trace elements (ppm) in stream sediments

Analyte	AKT 1	AKT 2	AKT 3	AKT 4	AKT 5	AKT 6	AKT 7	AKT 8	AKT 9	AKT 10	AKT 11	AKT 12	AKT 13	AKT 14	AKT 15
Ba	360.23	368.82	367.17	359.20	359.58	360.75	360.71	359.20	373.47	350.86	365.45	354.89	368.75	358.14	366.02
Co	4.15	4.10	3.92	3.91	3.82	4.16	4.12	3.91	3.87	3.90	4.05	4.20	3.88	4.14	3.95
Cr	479.12	479.52	472.42	419.69	475.12	489.92	470.28	489.69	481.29	473.06	474.32	486.75	462.11	479.58	471.92
Cs	1.95	1.90	1.94	2.08	2.02	1.96	2.06	2.08	1.92	2.05	2.08	1.96	2.10	1.88	2.03
Cu	13.19	13.08	12.45	12.48	12.41	13.61	12.68	13.48	12.69	12.44	12.91	13.45	12.36	13.02	12.77
Hf	6.28	6.27	6.23	6.25	5.89	6.18	5.88	6.25	5.83	5.86	6.14	6.39	5.91	6.07	5.85
Mo	7.97	7.70	8.17	7.69	8.05	7.80	8.08	7.69	8.28	8.31	8.20	7.59	8.34	7.72	8.05
Ni	16.97	17.84	16.33	15.61	17.30	17.70	17.14	16.61	17.47	17.29	17.42	16.88	17.55	16.24	17.39
Pb	11.94	12.47	12.44	12.13	12.28	11.86	11.91	12.13	12.27	12.42	12.36	11.95	12.44	12.09	12.27
Rb	210.00	155.00	180.00	158.00	160.00	130.00	200.00	170.00	175.00	190.00	175.18	162.33	185.20	168.94	178.55
Sc	2.18	2.01	2.09	2.03	2.11	2.03	2.04	2.03	2.17	2.15	2.07	2.18	2.01	2.09	2.15
Sr	54.20	58.25	54.82	48.08	58.33	55.62	57.77	58.08	55.10	58.69	56.92	54.78	59.04	55.36	57.15
Th	13.90	13.74	14.61	13.20	14.45	13.78	14.49	14.20	14.74	14.06	14.24	13.79	14.55	14.03	14.47
U	1.37	1.41	1.45	1.35	1.44	1.44	1.40	1.35	1.45	1.44	1.42	1.35	1.47	1.38	1.45
V	15.63	15.45	15.58	16.34	15.71	16.70	15.60	16.34	15.79	16.30	16.22	15.85	16.34	15.91	16.28
Y	9.51	9.76	10.28	9.76	10.08	10.48	9.78	9.76	9.55	10.19	9.94	10.23	9.81	10.14	9.87
Zn	15.26	15.21	14.91	15.75	15.23	14.47	15.69	15.75	14.67	14.56	15.14	14.83	15.31	14.92	15.21
Zr	247.47	247.84	260.54	230.95	256.16	241.51	261.88	240.95	250.15	261.68	254.85	243.92	258.14	247.76	252.88

Table 2: Descriptive analysis for the analyzed samples

Analyte	Min	Max	Mean	Median	STD	Threshold	
						Mean + 2SD	Median + 2SD
Ba	350.86	373.47	362.22	360.71	5.95	374.11	372.60
Co	3.82	4.20	4.01	3.95	0.13	4.26	4.21
Cr	419.69	489.92	473.65	475.12	16.72	507.10	508.57
Cs	1.88	2.10	2.00	2.02	0.07	2.15	2.17
Cu	12.36	13.61	12.87	12.77	0.42	13.71	13.61
Hf	5.83	6.39	6.09	6.14	0.20	6.48	6.53
Mo	7.59	8.34	7.98	8.05	0.26	8.49	8.57
Ni	15.61	17.84	17.05	17.29	0.62	18.28	18.52
Pb	11.86	12.47	12.20	12.27	0.21	12.62	12.69
Rb	130.00	210.00	173.21	175.00	19.51	212.24	214.02
Sc	2.01	2.18	2.09	2.09	0.06	2.22	2.21
Sr	48.08	59.04	56.15	56.92	2.76	61.66	62.44
Th	13.20	14.74	14.15	14.20	0.42	14.99	15.04
U	1.35	1.47	1.41	1.42	0.04	1.50	1.50
V	15.45	16.70	16.00	15.91	0.38	16.76	16.66
Y	9.51	10.48	9.94	9.87	0.28	10.50	10.43
Zn	14.47	15.75	15.13	15.21	0.41	15.94	16.02
Zr	230.95	261.88	250.45	250.15	8.83	268.11	267.81

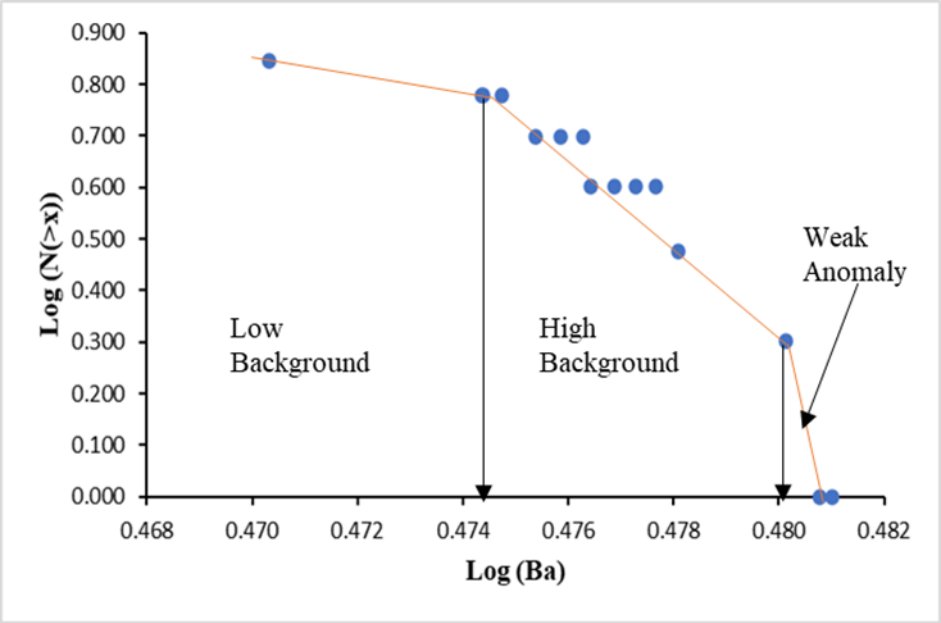

Fig. 2: Multifractal modeling of B

The first population ranges from 12.36ppm to 12.48ppm, indicating low background concentration. The second population ranges from 12.68ppm to 13.19ppm, reflecting high background concentration. The third population, ranges from 13.45ppm to 13.61ppm indicating a weak anomaly.

The C-N fractal modeling of Mo generated three statistical populations (Figure 4). The first ranges from 7.59ppm to 7.72ppm, indicating a low background concentration. The second population ranges from 7.80ppm to 8.28ppm, reflecting high background concentration. The third population, ranges from 8.31 ppm to 8.34ppm indicating a weak anomaly. The C-N fractal modeling of Ni produced three statistical populations (Figure 5). The first, ranges from 15.61ppm to 16.24ppm, indicating low background concentration. The second statistical population ranges from 16.33 ppm to

17.30ppm, indicating a high background concentration. The third population ranges from 17.39 ppm to 17.84 ppm, indicating a weak anomaly.

The C-N fractal analysis of Pb reveals three significant statistical populations (Figure 6). The first ranges from 11.86 ppm to 11.95ppm, indicating low background concentration. The second population ranges from 12.09 ppm to 12.36 ppm, reflecting a high background concentration. The third population ranges from 12.42ppm to 12.47 ppm, indicating a weak anomaly. The C-N fractal modeling of Th generated three statistical populations (Figure 7). The first ranges from 13.20ppm to 13.74ppm, indicating low background concentration. The second population ranges from 13.78 ppm to 14.45 ppm, indicating high background concentration. The third population ranges from 14.47ppm to 14.74ppm, reflecting a weak anomaly.

The C-N fractal analysis of U reveals three statistical populations (Figure 8). The first ranges from 1.35 ppm to 1.37ppm, reflecting low background concentration. The second population ranges from 1.38ppm to 1.44ppm, indicating high background concentration. The third population ranges from 1.45ppm to 1.47 ppm, reflecting a weak anomaly.

The C-N fractal modeling of Zn produced three statistical populations (Figure 9). The first ranges from 14.47 ppm to 14.92 ppm, reflecting low background concentration. The second population ranges from 15.14ppm to 15.31 ppm, indicating high background concentration. The third population ranges from 15.69 ppm to 15.75 ppm, indicating a weak anomaly. The classified anomaly and background map of Ba, Cu, Mo, Ni, Pb, Th, U, and Zn are shown in Figure 10, 11, 12, 13, 14, 15, 16, and 17 respectively.

4.3 Multivariate statistical analysis of data

4.3.1 Pearson correlation analysis (CA)

Prior to Pearson correlation analysis (CA), centered log ratio transformation (clr) was done to address the closure effect of compositional data. The result is given in Table 3. The CA of the stream sediment geochemical data revealed variable relationships among the trace elements (Table 4). Barium (Ba) exhibited positive correlations with Pb (r = 0.539), U (r = 0.382), Zn (r = 0.327), and Hf (r = 0.293), while showing weak to negative associations with Cr (r = –0.167), Cs (r = –0.099), and Rb (r = –0.400). Cobalt (Co) showed a strong positive correlation with Cu (r = 0.762) and Hf (r = 0.651), but was negatively correlated with Mo (r = –0.708) and Th (r = –0.633). Chromium (Cr) correlated positively with Cu (r = 0.587), Ni (r = 0.390), and Sr (r = 0.464), while displaying strong negative correlation with Cs (r = –0.645). Cesium (Cs) correlated negatively with Cr (r = –0.645) and Co (r = –0.324), but positively with V (r = 0.550) and Zn (r = 0.561). Copper (Cu) displayed strong positive correlations with Co (r = 0.762) and Hf (r = 0.725), and a strong negative correlation with Mo (r = –0.827) and Zr (r = –0.805).

Hafnium (Hf) was strongly positively correlated with Cu (r = 0.725) and Co (r = 0.651), while negatively correlated with Mo (r = –0.676) and Zr (r = –0.707). Molybdenum (Mo) exhibited strong negative correlations with Cu (r = –0.827), Co (r = –0.708), Hf (r = –0.676), and Zn (r = –0.337), but was positively correlated with U (r = 0.676) and Zr (r = 0.608). Nickel (Ni) showed moderate positive correlation with Sr (r = 0.569) and U (r = 0.452).

Lead (Pb) was positively correlated with Ba (r = 0.539) and U (r = 0.427), but negatively correlated with Co (r = –0.333) and Cr (r = –0.388). Rubidium (Rb) exhibited negative correlations with several elements including Cu (r = –0.564) and Y (r = –0.702), but a positive association with Zr (r = 0.398). Strontium (Sr) correlated positively with Cr (r = 0.464) and Ni (r = 0.569), while negatively correlated with Hf (r = –0.536).

Thorium (Th) showed a positive relationship with Mo (r = 0.518) and U (r = 0.472), but negative correlation with Co (r = –0.633) and Cu (r = –0.521). Uranium (U) was positively correlated with Mo (r = 0.676), Pb (r = 0.427), and Zr (r = 0.455). Vanadium (V) exhibited positive correlations with Cs (r = 0.550), Cu (r = 0.377), and Y (r = 0.483). Yttrium (Y) correlated positively with V (r = 0.483), Cu (r = 0.333), and Hf (r = 0.399), but showed strong negative correlation with Rb (r = –0.702).

Zinc (Zn) exhibited positive correlations with Cs (r = 0.561) and Ba (r = 0.327), but negative correlations with Cr (r = –0.496) and Ni (r = –

0.444). Zirconium (Zr) was strongly negatively correlated with Cu (r = –0.805) and Hf (r = –0.707), while positively correlated with Mo (r = 0.608), Th (r = 0.543), and U (r = 0.455).

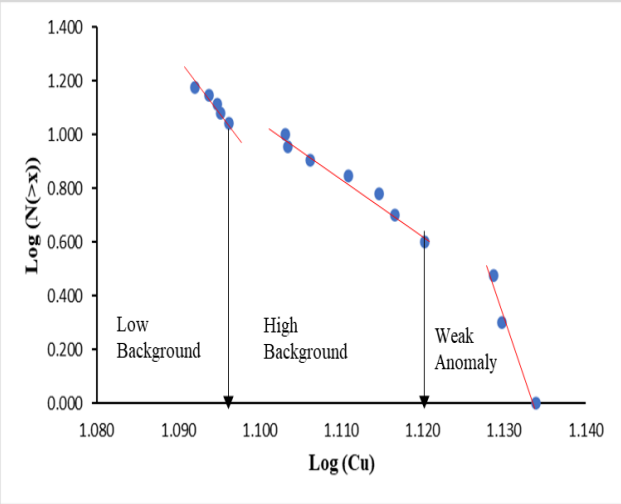

Fig. 3: Multifractal modeling of Cu

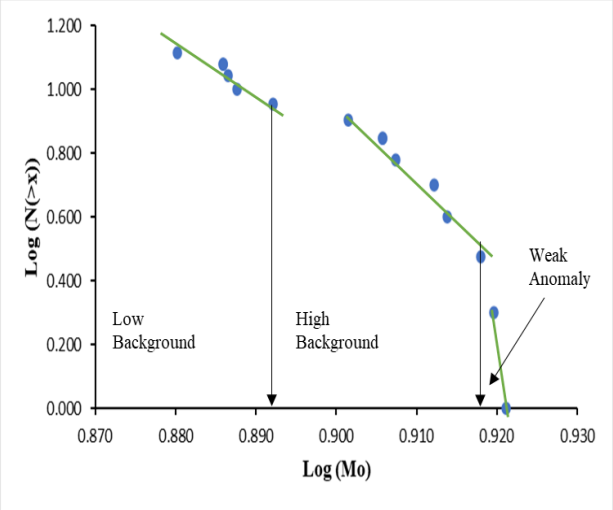

Fig. 4: Multifractal modeling of Mo

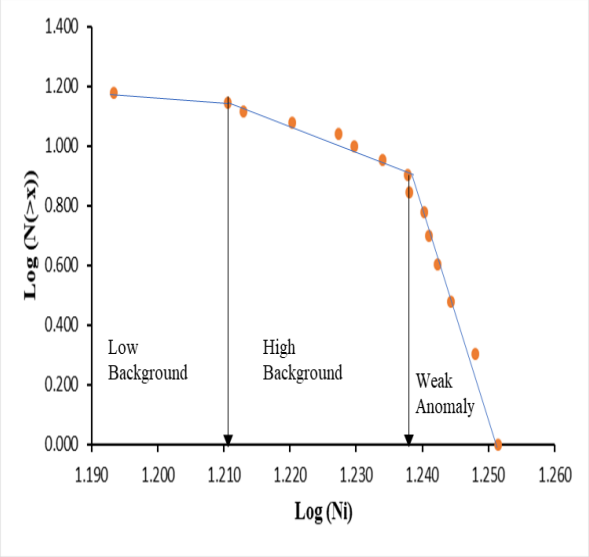

Fig. 5: Multifractal modeling of Ni

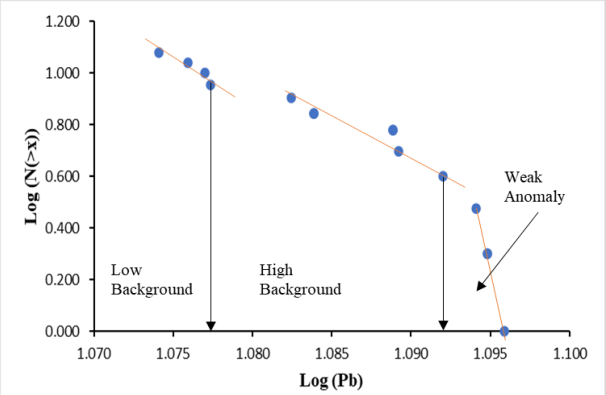

Fig. 6: Multifractal modeling of Pb

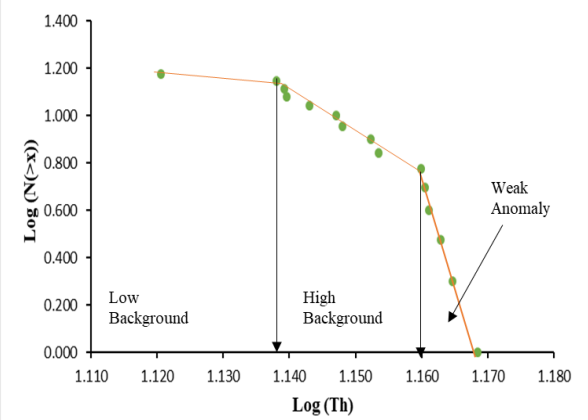

Fig. 7: Multifractal modeling of Th

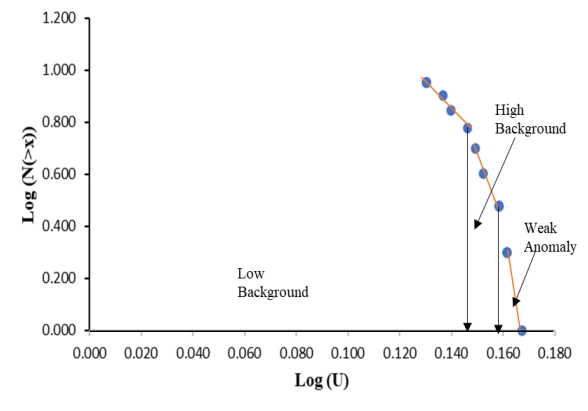

Fig. 8: Multifractal modeling of U

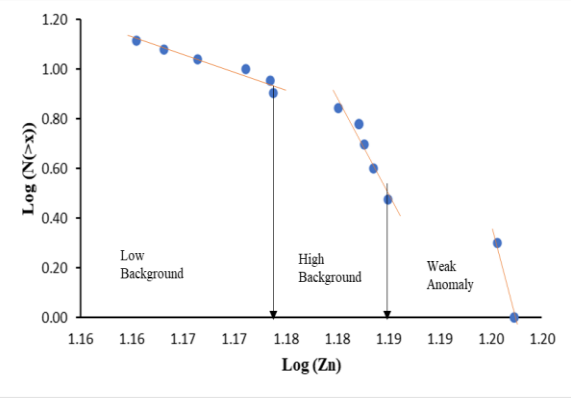

Fig. 9: Multifractal modeling of Zn

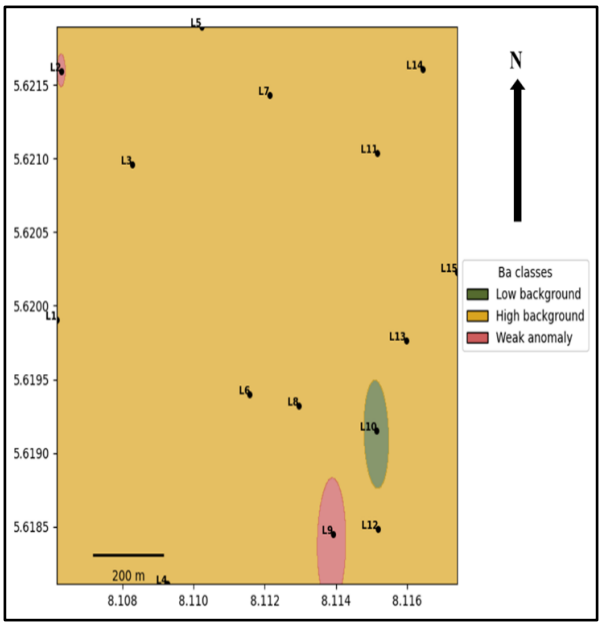

Fig.10: Classified anomaly and background map of Ba using fractal C–N model.

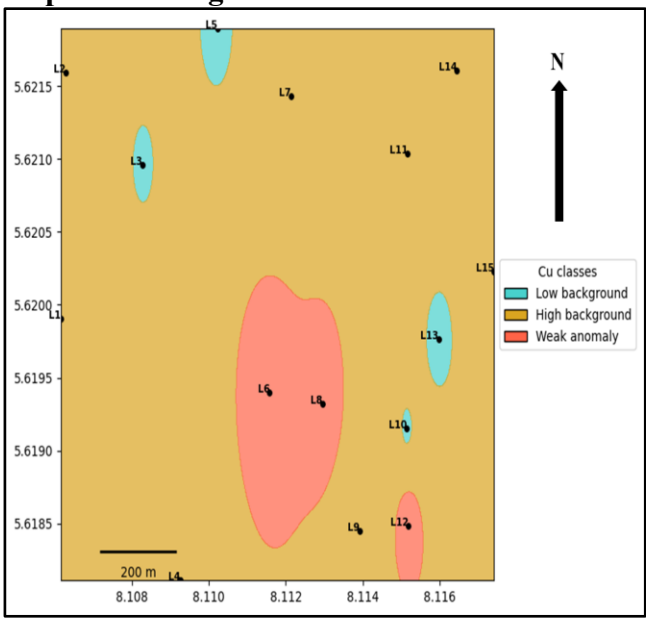

Fig.11: Classified anomaly and background map of Cu using fractal C–N model.

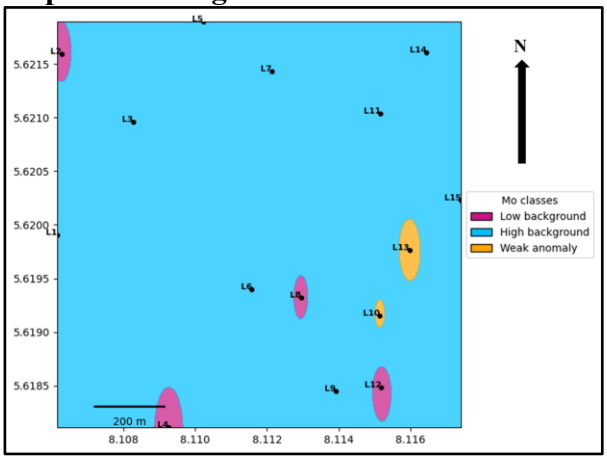

Fig.12: Classified anomaly and background map of Mo using fractal C–N model.

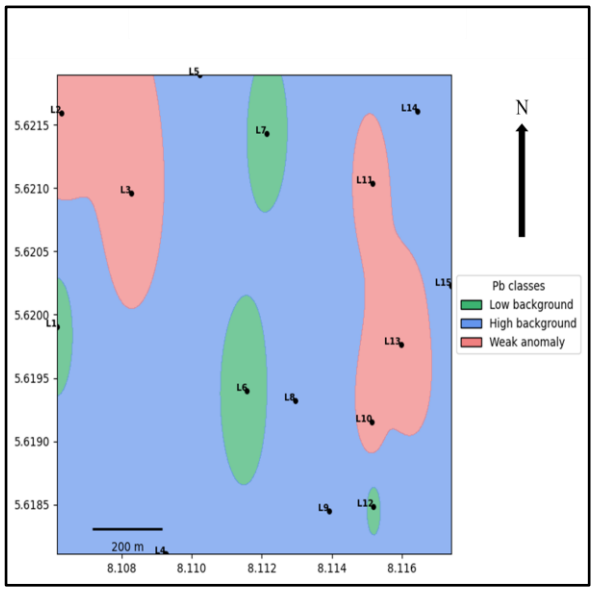

Fig.13: Classified anomaly and background map of Pb using fractal C–N model.

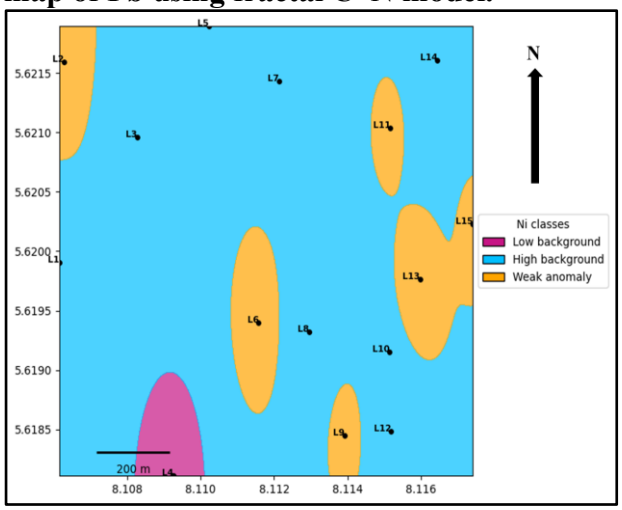

Fig.14: Classified anomaly and background map of Ni using fractal C–N model.

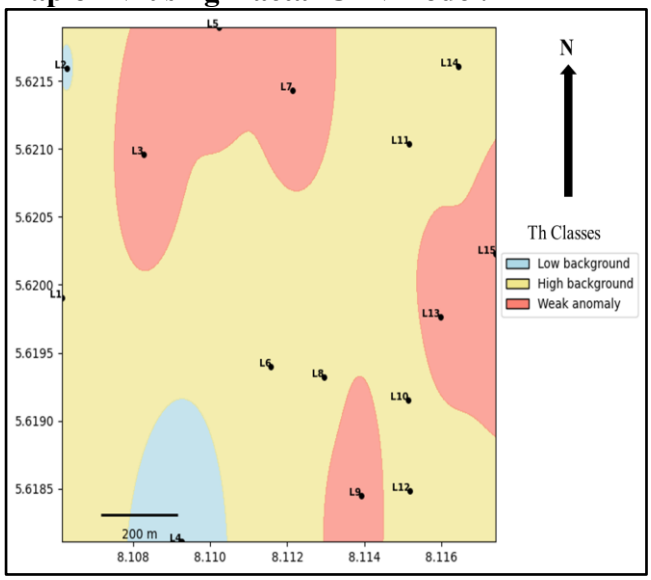

Fig.15: Classified anomaly and background map of Th using fractal C–N model.

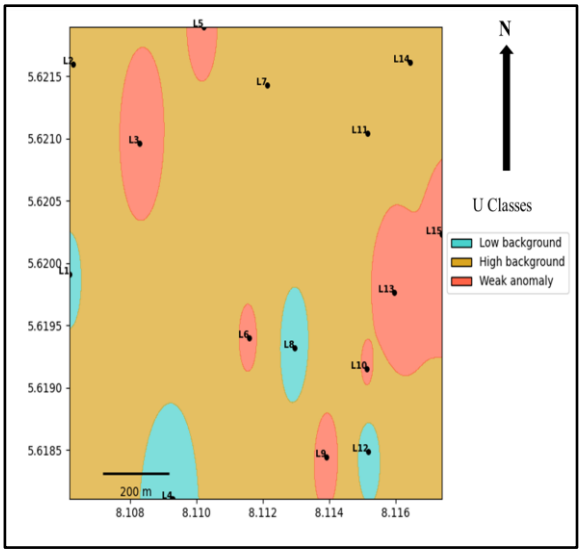

FIG.16: Classified anomaly and background map of U using fractal C–N model.

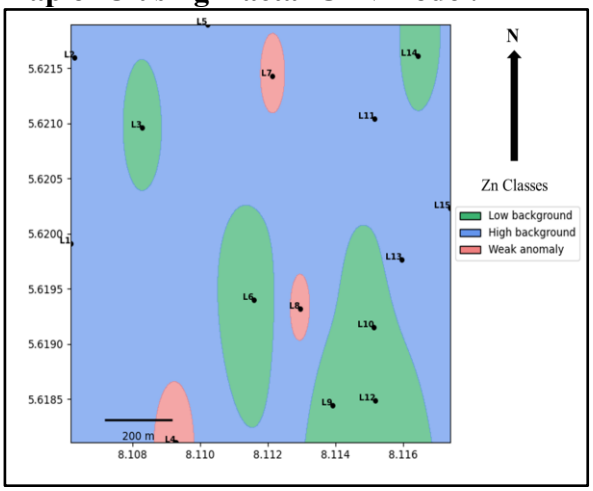

Fig.17: Classified anomaly and background map of Zn using fractal C–N model.

4.3.2 Principal component analysis (PCA)

The principal component analysis (PCA) extracted five major components with eigenvalues greater than 1, accounting for 83.02% of the total variance (Table 5). The first principal component (PC1) explained 28.82% of the total variance and showed strong positive loadings for Mo (0.913), Zr (0.806), U (0.684), and Th (0.641), with strong negative loadings for Cu (–0.924), Hf (–0.812), and Co (–0.800).

The second principal component (PC2), which accounted for 15.51% of the total variance, was dominated by strong positive loading of Cr (0.709) and moderate contributions from Sc (0.490) and Ni (0.308). A strong negative loading was observed for Cs (–0.937), while Zn (–0.714) also showed a significant negative contribution.

The third principal component (PC3) explained 13.34% of the variance and was characterized by strong positive loadings for Y (0.859) and V (0.726), while Rb (–0.726) contributed negatively. U (0.415) and Pb (0.242) also showed moderate positive loadings in this component.

The fourth principal component (PC4) accounted for 12.76% of the variance, with strong positive contributions from Sr (0.836) and Ni (0.740). Sc (–0.670) contributed negatively to this component.

The fifth principal component (PC5) explained 12.58% of the variance and was characterized by a very strong positive loading of Ba (0.975) and Pb (0.692), while Rb (–0.389) and Sr (–0.318) showed negative associations.

The scree plot (Figure 18) illustrates the distribution of eigenvalues across the principal components. The plot shows a steep decline from the first to the fourth component, after which the curve begins to level off. The first five components have eigenvalues greater than 1, indicating that they capture most of the variance in the dataset. This means that the data variability (83.016 total) is explained by PC1 (28.815), PC2 (15.513), PC3 (13.343), PC4 (12.761), and PC5 (12.583).

The biplot of PC1 vs. PC2 (Figure 19) illustrates the relationships among the analyzed elements and their contributions to the two major principal components. PC1 captures the largest variance in the dataset, while PC2 accounts for the second most significant variation. The Longer arrows mean stronger influence on the principal components. Strong positive loadings on PC1 are dominated by Mo, Zr, U, and Th indicating that these elements are strongly associated with one another and contribute significantly along the positive axis of PC1. Strong negative loadings on PC1 are mainly represented by Cu, Co, and Hf, suggesting a contrasting geochemical behavior to the elements with positive PC1 loadings.

Along PC2, significant positive loadings are shown by Cr, and Sc, which indicates their grouping and shared geochemical controls. On the negative axis of PC2, elements with significant negative loadings include Zn, and V, suggesting another distinct association.

Table 3: Centered log ratio (clr) transformation results for the analyzed samples

Analyte (ppm)	AKT 1	AKT 2	AKT 3	AKT 4	AKT 5	AKT 6	AKT 7	AKT 8	AKT 9	AKT 10	AKT 11	AKT 12	AKT 13	AKT 14	AKT 15
Ba	2.98	3.02	3.01	3.03	2.99	3.00	2.98	2.99	3.03	2.95	2.99	2.98	3.00	3.00	3.00
Co	-1.48	-1.48	-1.53	-1.50	-1.55	-1.46	-1.49	-1.53	-1.54	-1.55	-1.51	-1.46	-1.55	-1.46	-1.53
Cr	3.27	3.28	3.26	3.18	3.27	3.31	3.25	3.30	3.28	3.25	3.25	3.30	3.23	3.29	3.25
Cs	-2.24	-2.25	-2.24	-2.13	-2.19	-2.21	-2.18	-2.16	-2.24	-2.19	-2.17	-2.22	-2.17	-2.25	-2.20
Cu	-0.32	-0.32	-0.38	-0.33	-0.38	-0.27	-0.37	-0.29	-0.36	-0.39	-0.35	-0.29	-0.39	-0.32	-0.36
Hf	-1.07	-1.05	-1.07	-1.03	-1.12	-1.06	-1.14	-1.06	-1.13	-1.14	-1.09	-1.04	-1.13	-1.08	-1.14
Mo	-0.83	-0.85	-0.80	-0.82	-0.81	-0.83	-0.82	-0.86	-0.78	-0.79	-0.80	-0.86	-0.79	-0.84	-0.82
Ni	-0.07	-0.01	-0.11	-0.11	-0.04	-0.01	-0.07	-0.09	-0.04	-0.06	-0.05	-0.06	-0.04	-0.10	-0.05
Pb	-0.42	-0.37	-0.38	-0.36	-0.39	-0.41	-0.43	-0.40	-0.39	-0.39	-0.39	-0.41	-0.39	-0.39	-0.40
Rb	2.44	2.15	2.29	2.20	2.18	1.98	2.39	2.24	2.27	2.34	2.26	2.20	2.31	2.24	2.28
Sc	-2.12	-2.19	-2.16	-2.15	-2.15	-2.18	-2.19	-2.19	-2.12	-2.14	-2.18	-2.11	-2.21	-2.15	-2.14
Sr	1.09	1.18	1.10	1.01	1.17	1.13	1.15	1.17	1.11	1.17	1.13	1.11	1.17	1.13	1.14
Th	-0.27	-0.27	-0.22	-0.28	-0.22	-0.26	-0.23	-0.24	-0.21	-0.26	-0.25	-0.27	-0.23	-0.24	-0.23
U	-2.59	-2.55	-2.53	-2.56	-2.53	-2.52	-2.57	-2.60	-2.52	-2.54	-2.56	-2.59	-2.52	-2.56	-2.53
V	-0.15	-0.15	-0.15	-0.06	-0.14	-0.07	-0.16	-0.10	-0.14	-0.12	-0.12	-0.13	-0.12	-0.12	-0.11
Y	-0.65	-0.61	-0.57	-0.58	-0.58	-0.53	-0.63	-0.62	-0.64	-0.59	-0.61	-0.57	-0.63	-0.57	-0.61
Zn	-0.18	-0.17	-0.20	-0.10	-0.17	-0.21	-0.15	-0.14	-0.21	-0.23	-0.19	-0.19	-0.18	-0.18	-0.18
Zr	2.61	2.62	2.66	2.58	2.65	2.60	2.66	2.59	2.63	2.66	2.63	2.61	2.64	2.63	2.63

Table 4: Pearson's correlation matrix

	Ba	*Co*	*Cr*	*Cs*	*Cu*	*Hf*	*Mo*	*Ni*	*Pb*	*Rb*	*Sc*	*Sr*	*Th*	*U*	*V*	*Y*	*Zn*	*Zr*
Ba	1.000																	
Co	0.051	1.000																
Cr	-0.167	0.323	1.000															
Cs	-0.099	-0.324	**-0.645**	1.000														
Cu	0.130	**0.762**	**0.587**	-0.193	1.000													
Hf	0.293	**0.651**	0.118	-0.030	**0.725**	1.000												
Mo	0.067	**-0.708**	-0.483	0.157	**-0.827**	**-0.676**	1.000											
Ni	0.104	0.002	0.390	-0.224	0.082	-0.301	0.088	1.000										
Pb	**0.539**	-0.333	-0.388	0.125	-0.255	0.178	0.230	-0.071	1.000									
Rb	-0.400	-0.318	-0.373	0.016	**-0.564**	-0.413	0.335	-0.407	-0.292	1.000								
Sc	-0.120	0.120	0.140	-0.333	0.126	0.092	-0.046	-0.190	-0.099	0.118	1.000							
Sr	-0.384	-0.322	**0.464**	-0.155	-0.189	**-0.536**	0.010	**0.569**	-0.141	-0.048	-0.442	1.000						
Th	0.186	**-0.633**	0.089	-0.176	**-0.521**	**-0.636**	**0.518**	0.024	0.001	0.174	-0.069	0.313	1.000					
U	0.382	-0.449	-0.138	-0.095	**-0.473**	**-0.461**	**0.676**	**0.452**	0.427	-0.328	-0.160	0.191	**0.472**	1.000				
V	0.172	0.117	-0.186	**0.550**	0.377	0.298	-0.099	-0.068	0.216	**-0.569**	-0.063	-0.327	-0.367	0.112	1.000			
Y	-0.035	0.350	0.202	-0.033	0.333	0.399	-0.245	-0.092	0.189	**-0.702**	0.083	-0.127	-0.227	0.217	**0.483**	1.000		
Zn	0.327	0.090	**-0.496**	**0.561**	0.134	0.400	-0.337	-0.444	0.203	0.035	-0.265	-0.379	-0.234	-0.419	0.214	-0.182	1.000	
Zr	-0.330	**-0.478**	-0.124	-0.188	**-0.805**	**-0.707**	**0.608**	0.100	-0.001	0.398	-0.176	**0.476**	0.543	**0.455**	**-0.600**	-0.076	**-0.455**	1

Table 5: Principal component analysis

Variable	Component				
	PC1	PC2	PC3	PC4	PC5
Ba	-0.110	0.010	-0.024	0.001	0.975
Co	-0.800	0.252	0.141	-0.108	-0.083
Cr	-0.380	0.709	0.083	0.433	-0.206
Cs	0.086	-0.937	0.165	-0.019	-0.096
Cu	-0.924	0.188	0.241	0.095	0.014
Hf	-0.812	-0.051	0.193	-0.289	0.256
Mo	0.913	-0.073	0.016	-0.106	0.140
Ni	0.085	0.308	0.155	0.740	0.097
Pb	0.226	-0.213	0.242	-0.098	0.692
Rb	0.358	-0.102	-0.726	-0.373	-0.389
Sc	-0.050	0.490	0.098	-0.670	-0.120
Sr	0.264	0.157	-0.096	0.836	-0.318
Th	0.641	0.250	-0.264	0.177	0.210
U	0.684	0.168	0.415	0.254	0.456
V	-0.242	-0.476	0.726	-0.052	0.132
Y	-0.173	0.132	0.859	-0.088	-0.015
Zn	-0.402	-0.714	-0.306	-0.150	0.301
Zr	0.806	0.209	-0.153	0.140	-0.233
Total	5.187	2.792	2.402	2.297	2.265
% of Variance	28.815	15.513	13.343	12.761	12.583
Cumulative %	28.815	44.329	57.672	70.433	83.016

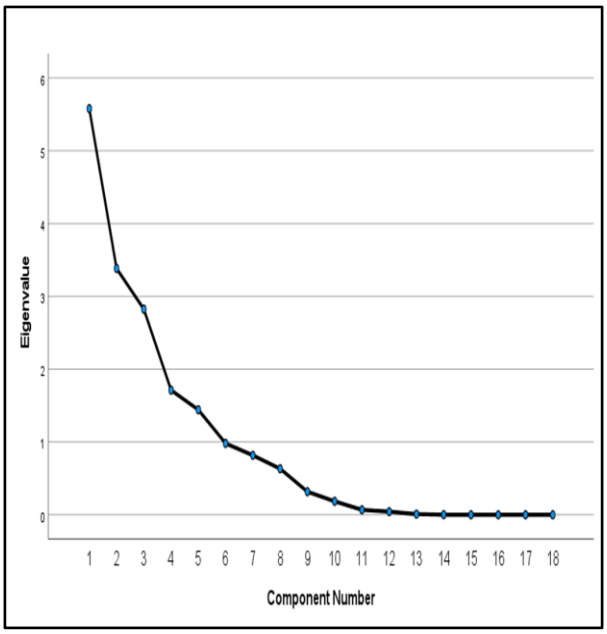

Fig.18: Scree plot of PCA

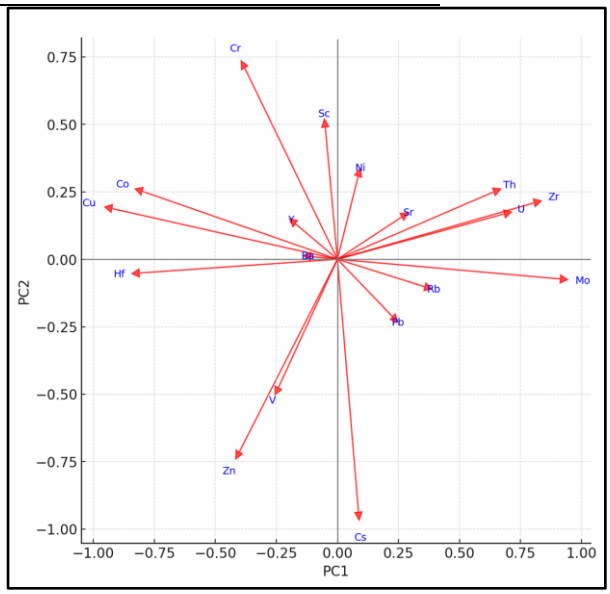

Fig. 19: Biplot of PC1 vs. PC2

3.2 Discussion

3.2.1 Concentration of trace element in sediment

The concentrations of trace elements in stream sediments from the Akpet area provide insights into the geochemical characteristics and possible processes influencing sediment composition. Comparisons with upper continental crust (UCC) reference values (Taylor & McLennan, 1985; Rudnick, 2005) reveal patterns of enrichment and depletion that reflect contributions from felsic and mafic lithologies.

Barium (Ba) concentrations are slightly depleted relative to UCC, suggesting limited feldspar input or preferential leaching during weathering. Cobalt (Co) is strongly depleted, which is consistent with the limited contribution from mafic or ultramafic rocks, as Co is typically enriched in such lithologies (Taylor & McLennan, 1985).

Chromium (Cr) shows marked enrichment relative to UCC, with values nearly five times higher than the global average. This enrichment likely reflects inputs from mafic or ultramafic sources, as Cr is commonly hosted in ferromagnesian minerals such as chromite, pyroxene, and amphibole (Taylor & McLennan, 1985).

Cesium (Cs) and rubidium (Rb) are both enriched compared to UCC, reflecting felsic provenance. Their association with K-bearing minerals (micas, K-feldspar) indicates derivation from granitic rocks. This enrichment contrasts with the depletion observed in Sr, suggesting extensive removal of plagioclase, which hosts much of the Sr in primary igneous rocks (Taylor & McLennan, 1985; McLennan, 1993).

Copper (Cu) and nickel (Ni) are depleted relative to UCC, also confirming the limited contribution of ultramafic rocks to the sediments. Their low values, along with the strong enrichment of Cr, suggest geochemical contributions, where Cr-bearing phases are more resistant to weathering than Cu- and Ni-bearing minerals.

Lead (Pb) and zinc (Zn) are both depleted, with concentrations well below UCC averages. This indicates minimal anthropogenic influence, as these metals are often enriched in areas affected by industrial or mining activity (Förstner & Wittmann, 2012).

High field strength elements (HFSEs: Zr, Hf, Th, and U) display moderate enrichment. The elevated Zr and Hf contents are consistent with the presence of detrital zircon, while the enrichment in Th reflects contributions from accessory minerals such as monazite. Uranium, however, remains close to UCC levels, suggesting limited secondary mobility under present redox conditions (Taylor & McLennan, 1985). These enrichments point toward felsic lithologies as dominant sediment sources.

Transition metals such as vanadium (V) and scandium (Sc) are strongly depleted compared to UCC, and this support the limited influence of mafic or ultramafic rocks. Yttrium (Y) concentrations are also low, consistent with limited heavy rare earth element (HREE) enrichment in the sediments.

Strontium (Sr) concentrations are depleted, nearly six times lower than UCC values. This depletion reflects the weathering of feldspar, where Sr is preferentially leached relative to more resistant elements such as Rb and Cs.

3.2.2 Multivariate statistical analysis of data

Pearson correlation analysis is a widely used statistical method for assessing the strength and direction of linear relationships between two continuous variables. It is expressed through the correlation coefficient (r), which ranges between –1 and +1. A positive correlation ($r \rightarrow +1$) indicates that as the concentration of one element increases, the other also increases, suggesting that the elements may share similar geochemical controls or originate from common sources. In contrast, a negative correlation ($r \rightarrow -1$) signifies that as one element increases, the other decreases, which may reflect contrasting geochemical affinities. A correlation coefficient close to 0 suggests the absence of a significant linear relationship between the variables (Davis & Sampson, 1986; Reimann & Filzmoser, 2000). In geochemical studies, Pearson correlation analysis is often applied to identify elemental associations that provide insights into lithological control, weathering processes, mineralization, or anthropogenic influences (Rollinson, 2014; Reimann *et al*., 2011). Such relationships are essential for reducing data complexity and for revealing geochemical trends (Aitchison, 1982; Filzmoser *et al*., 2009).

The Pearson correlation analysis (CA), following centered log-ratio (clr) transformation to mitigate closure effects (Aitchison, 1982; Pawlowsky-Glahn & Buccianti, 2011), revealed distinct geochemical associations among the analyzed elements.

Barium (Ba) displayed positive correlations with Pb, U, Zn, and Hf, suggesting its association with accessory minerals such as barite or feldspar, often linked with felsic provenance (McLennan, 1993). The negative correlation between Ba and Rb implies differing geochemical behavior during weathering, as Rb is typically enriched in K-feldspar and micas while Ba is preferentially leached (Taylor & McLennan, 1985).

Cobalt (Co) and copper (Cu) showed a strong positive correlation ($r = 0.762$), indicating possible derivation from mafic mineral phases such as sulfides or ferromagnesian silicates (Kabata-Pendias, 2000). Their strong positive relationship with hafnium (Hf) is somewhat unusual, but may reflect the co-occurrence of trace Hf-bearing zircons with sulfide-rich phases in mixed sediment inputs. Negative correlations of Co and Cu with molybdenum (Mo) and thorium (Th) highlight contrasting geochemical controls, with Mo and Th often enriched in felsic rocks, whereas Co and Cu are more characteristic of mafic contributions (Rudnick, 2005).

Chromium (Cr) correlated positively with Cu, Ni, and Sr, supporting a mafic or ultramafic source influence. The strong negative correlation with cesium (Cs) reflects their contrasting geochemical affinities: Cr with mafic ferromagnesian minerals, and Cs with felsic K-bearing phases (McLennan, 1993). Similarly, Ni showed positive correlation with Sr, reflecting shared association with mafic minerals and less weathered inputs.

Cesium (Cs) correlated positively with vanadium (V) and zinc (Zn), suggesting adsorption onto clay minerals during weathering (Förstner & Wittmann, 2012). The negative correlation between Cs and Cr supports the felsic–mafic contrast in sediment provenance.

Molybdenum (Mo) displayed strong positive correlations with U and Zr, which points toward felsic provenance and association with accessory minerals like zircon and uraninite. Its negative correlation with Cu, Co, and Hf again reveals a felsic–mafic partitioning of geochemical signatures.

Lead (Pb) was positively associated with Ba and U, reflecting shared occurrence in felsic mineral assemblages and resistance to leaching (Rudnick, 2005). The negative relationship with Co and Cr indicates a lack of mafic input control. Similarly, Th–Mo and Th–U positive correlations highlight felsic contributions, as these elements concentrate in accessory minerals like monazite and zircon (McLennan, 1993).

Rubidium (Rb) showed strong negative correlation with Y, and weaker negative correlations with Cu, consistent with Rb's felsic affinity and the tendency of Y to concentrate in accessory phases within more mafic or intermediate lithologies (Taylor & McLennan, 1985).

Vanadium (V) and yttrium (Y) both showed positive associations, reflecting their compatibility with heavy minerals and possible substitution in ferromagnesian silicates (Kabata-Pendias, 2000). The positive correlation of Y with Cu and Hf also suggests links to heavy mineral fractions.

Zinc (Zn) correlated positively with Cs and Ba, consistent with adsorption onto clays and possible association with feldspar-rich lithologies. Its negative correlation with Cr and Ni confirms its detachment from mafic input signatures. Zirconium (Zr), on the other hand, showed strong positive correlations with Mo, Th, and U, consistent with zircon-bearing felsic contributions (McLennan, 1993), and strong negative correlation with Cu and Hf, highlighting contrasting source influences.

Specifically, the correlation analysis reveals two dominant geochemical associations: (i) a felsic-related suite (Rb, Cs, Th, U, Zr, Mo, Pb, Ba, Zn) reflecting input from granitic rocks, and (ii) a mafic-related suite (Cr, Co, Cu, Ni, V, Sr, Hf, Y), linked to ferromagnesian silicates and sulfides. These associations reflect the mixed provenance of the Akpet sediments, with felsic sources dominating but with little mafic/ultramafic contributions.

Principal component analysis (PCA) is also a widely used multivariate statistical technique that reduces the dimensionality of geochemical datasets while retaining the most significant variance present in the data (Jolliffe & Cadima,

2016). PCA highlights geochemical associations and assists in discriminating lithological sources, weathering trends, and mineralization signatures (Reimann *et al*., 2011; Filzmoser *et al*., 2009). The eigenvalues reflect the relative importance of each component, while the loadings provide insight into the geochemical affinities of elements and their potential sources (Davis, 2018).

PCA has been successfully applied to distinguish between felsic and mafic provenance, identify mineralization-related anomalies, and unravel compositional controls in sediments and soils (Carranza, 2008; Kong *et al*., 2022). Thus, in the present study, PCA provides a framework for grouping trace elements into geochemically meaningful associations that reflect provenance and mineralization potential.

The PCA extracted five components with eigenvalues greater than 1, accounting for 83.02% of the total variance, which demonstrates a strong representation of the geochemical dataset.

PC1 (28.82% of variance), dominated by strong positive loadings of Mo, Zr, U, and Th, and strong negative loadings of Cu, Hf, and Co. The positive loadings suggest felsic-related geochemical inputs, as Mo, U, Th, and Zr are enriched in accessory minerals such as zircon, uraninite, and monazite, typically associated with granitic lithologies (McLennan, 1993; Rudnick, 2005). Conversely, the negative association of Cu, Co, and Hf reflects input of mafic/ultramafic compositions, as these elements occur in ferromagnesian silicates (Kabata-Pendias, 2000). PC2 (15.51% of variance), shows strong positive loadings of Cr and Sc, and a moderate contribution from Ni, indicate mafic or ultramafic inputs, as these elements are compatible with ferromagnesian minerals and less mobile during weathering. The strong negative loadings of Cs and Zn, elements often enriched in felsic minerals and adsorbed onto clays. PC3 (13.34% of variance), characterized by strong positive loadings of Y and V, along with moderate positive contributions from U and Pb. These associations may reflect the role of heavy minerals such as zircon and monazite, which host U and Pb, alongside substitution of Y and V in accessory minerals (Förstner & Wittmann, 2012). The strong negative loading of Rb points to its felsic control. PC4 (12.76% of variance), dominated by Sr and Ni, with a negative contribution from Sc, this component likely reflects inputs from feldspar-bearing lithologies, where Sr substitutes for Ca, and Ni reflects minor mafic contributions (Taylor & McLennan, 1985). The negative loading of Sc further indicates mixed compositions. PC5 (12.58% of variance), defined by very strong positive loading of Ba and Pb, with negative associations from Rb and Sr, this component may represent feldspar- and barite-related signatures (Ba enrichment), alongside Pb possibly hosted in sulfide phases (McLennan, 1993). The negative Rb suggests contrasting controls between alkali feldspar and barite/Pb-bearing minerals like galena.

he scree plot confirms the significance of the first five components, explaining over 83% of the variance, while the biplot of PC1 vs. PC2 clearly differentiates felsic-associated elements (Mo, U, Th, Zr) from mafic-related elements (Cu, Co, Cr, Ni, Sc). This highlights both felsic and mafic inputs, and mineralization signatures like sulfide-related Cu–Co association and felsic accessory phases hosting U–Th–Zr–Mo.

3.2.3 Fractal/multifractal modeling analysis

Fractal models are increasingly applied in geochemical exploration because geochemical data typically display self-similarity and scale invariance, which conventional statistical methods may not adequately capture (Cheng *et al*., 1994; Agterberg, 2012). Among these, the Concentration–Number (C–N) model provides an effective approach for separating geochemical populations into distinct thresholds that define background and anomalous concentrations (Cheng, 1995). The principle of the C–N method is that when geochemical concentrations are plotted against their cumulative number on a log–log scale, breaks in slope reflect different geochemical populations (Carranza, 2008). These populations typically correspond to background levels, thresholds, and anomalies, which are critical in mineral exploration since they distinguish natural lithological contributions from mineralization-related enrichment (Soto-Jiménez & Páez-Osuna, 2010).

In this study, C–N fractal modeling was applied to Ba, Cu, Mo, Ni, Pb, Th, U, and Zn in order to

establish geochemical thresholds and delineate anomalous zones. The results reveal three main statistical populations for each element, corresponding to low background, high background, and weak anomaly.

For Ba, the first population (350.86–354.89 ppm) represents the low background, while the second (358.14–368.75 ppm) reflects high background, and the third (368.82–373.47 ppm) defines a weak anomaly. The transition from background to anomaly suggests limited Ba enrichment, possibly linked to feldspar alteration or minimal barite mineralization (Kabata-Pendias, 2000).

In the case of Cu, three populations were also identified: low background (12.36–12.48 ppm), high background (12.68–13.19 ppm), and weak anomaly (13.45–13.61 ppm). The weak anomaly suggests little/no Cu enrichment, which may represent early-stage sulfide mineralization rather than widespread ore accumulation (Reimann & Garrett, 2005).

Mo displayed low background values between 7.59–7.72 ppm, high background between 7.80–8.28 ppm, and weak anomaly between 8.31–8.34 ppm. The presence of anomalous Mo, even at weak levels, is noteworthy as Mo is often associated with hydrothermal systems and granitic-related mineralization (McLennan, 1993; Rudnick, 2005).

For Ni, three populations were identified: low background (15.61–16.24 ppm), high background (16.33–17.30 ppm), and weak anomaly (17.39–17.84 ppm). The weak anomaly could be indicative of contributions from mafic lithologies or weathered ultramafic inputs, where Ni typically occurs in ferromagnesian minerals.

Pb produced three populations: low background (11.86–11.95 ppm), high background (12.09–12.36 ppm), and weak anomaly (12.42–12.47 ppm). Lead anomalies may be linked to sulfide mineralization, particularly galena or secondary dispersion from Pb-bearing accessory minerals (Förstner & Wittmann, 2012).

For Th, populations were defined as low background (13.20–13.74 ppm), high background (13.78–14.45 ppm), and weak anomaly (14.47–14.74 ppm). Thorium anomalies are typically associated with accessory minerals such as monazite and thorite, reflecting felsic lithological controls rather than direct mineralization potential (Taylor & McLennan, 1985).

U exhibited three populations: low background (1.35–1.37 ppm), high background (1.38–1.44 ppm), and weak anomaly (1.45–1.47 ppm). The presence of anomalous U may indicate localised enrichment in heavy minerals such as zircon or uraninite, consistent with a felsic provenance (Rudnick, 2005).

Lastly, Zn displayed three populations: low background (14.47–14.92 ppm), high background (15.14–15.31 ppm), and weak anomaly (15.69–15.75 ppm). Zinc anomalies may reflect sulfide mineralization, particularly sphalerite, though the weak anomaly suggests limited hydrothermal input (Kabata-Pendias, 2000).

The classified anomaly and background maps (Figures 9–16) spatially depict these thresholds, with anomalous populations outlining localized zones of enrichment. These weak anomalies across multiple elements (Ba, Cu, Mo, Ni, Pb, Th, U, and Zn) indicate minimal geochemical signals that may point toward early-stage or distal mineralization processes rather than widespread ore-forming systems.

4.0 Conclusion

Stream sediment geochemistry has proven valuable in narrowing potential mineral targets and providing a first-level guide for further exploration. For this study, a total of fifteen (15) stream sediment samples were systematically collected from active stream and river channels within the Akpet area. These samples were analyzed for trace elements using ICP-MS. In the Akpet area, trace elements such as Mo, U, Th, and Zr were found at anomalous concentrations above background levels, reflecting possible geochemical enrichment. The weak inter-element correlations and principal component analysis among base metals (Cu, Pb, Zn, and Ni) suggest lithological controls, not necessarily localized sulfide mineralization. Complementing this, the C–N fractal model effectively separated geochemical data into low background, high background, and weakly anomalous populations for Ba, Cu, Mo, Ni, Pb, Th, U, and Zn. Notably, Mo, U, and Th displayed higher anomalous thresholds compared to other elements, highlighting possible radioactive mineralization in the area.

Acknowledgement

The authors would like to acknowledge all the authors for their contribution to ensuring the successful completion of this research work.

5.0 References

Adekoya, J. A. (2003). Environmental effect of solid minerals mining. *Journal of Physical Sciences, Kenya*, *1*, 625-640.

Afzal, P., Fadakar, Y., Khakzad, A., Moarefvand, P., RASHIDNEZHAD, O. N., & ASADI, H. H. (2010). Separation of Geochemical Anomalies from Background by Using of Power Spectral-Area Fractal Method, Case Study: Kahang Porphyry Cu-Mo Deposit, Isfahan.

Agterberg, F. P. (2012). Multifractals and geostatistics. *Journal of Geochemical Exploration*, *122*, 113-122.

Aitchison, J. (1982). The statistical analysis of compositional data. *Journal of the Royal Statistical Society: Series B (Methodological)*, *44*(2), 139-160.

Carranza, E. J. M. (2008). *Geochemical anomaly and mineral prospectivity mapping in GIS*. Elsevier.

Cheng, Q. (1995). *Multifractal modelling and spatial analysis with GIS: Gold potential estimation in the Mitchell-Sulphurets area, northwestern British Columbia*. University of Ottawa (Canada).

Cheng, Q., Agterberg, F. P., & Ballantyne, S. B. (1994). The separation of geochemical anomalies from background by fractal methods. *Journal of Geochemical Exploration*, 51(2), 109–130.

Davis, J. C. (2018). Electrofacies in reservoir characterization. In *Handbook of Mathematical Geosciences: Fifty Years of IAMG* (pp. 211-223). Cham: Springer International Publishing.

Davis, J. C., & Sampson, R. J. (1986). *Statistics and data analysis in geology* (Vol. 646). New York: Wiley.

Ekwueme, B. N. (2003). The Precambrian geology and evolution of the Southeastern Nigerian basement complex.

Esmaeili, A., Moore, F., Keshavarzi, B., Jaafarzadeh, N., & Kermani, M. (2014). A geochemical survey of heavy metals in agricultural and background soils of the Isfahan industrial zone, Iran. *Catena*, *121*, 88-98.

Filzmoser, P., Hron, K., & Reimann, C. (2009). Principal component analysis for compositional data with outliers. *Environmetrics: The Official Journal of the International Environmetrics Society*, *20*(6), 621-632.`

Förstner, U., & Wittmann, G. T. W. (2012). *Metal pollution in the aquatic environment*. Springer Science & Business Media.

Garba, I. (2003). Geochemical discrimination of newly discovered rare-metal bearing and barren pegmatites in the Pan-African (600±150 Ma) basement of northern Nigeria. *Applied Earth Science*, *112*(3), 287-292.

Govett, G. J. S. (1983). *Handbook of exploration geochemistry: Rock geochemistry in mineral exploration* (Vol. 3). Elsevier.

Govett, G. J. S. (Ed.). (2013). *Rock geochemistry in mineral exploration* (Vol. 3). Elsevier.

Griffiths, J. C. (1967). *Scientific method in analysis of sediments*. McGraw-Hill.

Hawkes, H. E., & Webb, J. S. (1962). Geochemistry in mineral exploration.

Helsel, D. R. (2011). *Statistics for censored environmental data using Minitab and R* (Vol. 77). John Wiley & Sons.

Kabata-Pendias, A. (2000). *Trace elements in soils and plants*. CRC press.

Kong, Y., Chen, G., Liu, B., Xie, M., Yu, Z., Li, C., ... & Tang, R. (2022). 3D mineral prospectivity mapping of Zaozigou gold deposit, west Qinling, China: Machine learning-based mineral prediction. *Minerals*, *12*(11), 1361.

McLennan, S. M. (1993). Weathering and global denudation. *Journal of Geology*, 101(2), 295–303.

Obaje, N. G. (2009). *Geology and mineral resources of Nigeria* (Vol. 120, p. 221). Berlin: Springer.

Olade, M. A. (2021). Overview of Nigeria's Mineral Resources in the Context of Africa's Mineral Wealth.

Omang, B. O., Morphy, M. I., Amah, G., Tijani, O. L., Arikpo, T. O., & Kave, G. T. (2024). Major And Trace Element Geochemistry Of Pegmatites In Umai, Oban Massif, Se, Nigeria: Constraints On Their

Characterization And Mineralization Potential. *Global Journal of Geological Sciences*, *22*(1), 125-145.

Omang, B. O., Kave, G.T., Effiom,H.F.,Njoku, A.K., Odey, J.U. (2026). Comparative Assessment of Granite-Hosted Pegmatite-Quartz Veins in Akpet and Betem as a Potential for High Purity Quartz Resource. *Applied Sciences, Computing and Energy*, *4*(1), 12-154.

Oyawoye, M. O. (1964). The geology of the Nigerian Basement Complex-A survey of our present knowledge of them. *Journal of the Nigerian mining, geological and metallurgical Society*, *1*(2), 87-102.

Pawlowsky-Glahn, V., & Buccianti, A. (2011). *Compositional Data Analysis: Theory and Applications*. Chichester, UK: John Wiley & Sons.

Reimann, C., & Filzmoser, P. (2000). Normal and lognormal data distribution in geochemistry: Death of a myth. *Consequences for the statistical treatment of geochemical and environmental data*. *Environmental Geology*, 39(9), 1001–1014.

Reimann, C., & Garrett, R. G. (2005). Geochemical background—concept and reality. *Science of the total environment*, *350*(1-3), 12-27.

Reimann, C., Filzmoser, P., & Garrett, R. G. (2002). Factor analysis applied to regional geochemical data: Problems and possibilities. *Applied Geochemistry*, 17(3), 185–206.

Reimann, C., Filzmoser, P., Garrett, R., & Dutter, R. (2011). *Statistical data analysis explained: applied environmental statistics with R*. John Wiley & Sons.

RL, R. (2005). Composition of the continental crust. *The Crust, Treatise on Geochemistry*, *3*, 17-18.

Salminen, R., Chekushin, V., Tenhola, M., Bogatyrev, I., Gregorauskiene, V., Fedotova, E., ... & Zhdanova, L. (2005). *Geochemical atlas of eastern Barents region*. Gulf Professional Publishing.

Salminen, R., De Vos, W., & Tarvainen, T. (2006). *Geochemical atlas of Europe*. Espoo, Finland: Geological survey of Finland.

Smith, D. B., Cannon, W. F., Woodruff, L. G., Garrett, R. G., Klassen, R., Kilburn, J. E., ... & Morrison, J. M. (2005). *Major- and trace-element concentrations in soils from two continental-scale transects of the United States and Canada*. U. S. Geological Survey.

Soto-Jiménez, M. F., & Páez-Osuna, F. (2010). A first approach to study the mobility and behavior of lead in hypersaline salt marsh sediments: Diffusive and advective fluxes, geochemical partitioning and Pb isotopes. *Journal of Geochemical Exploration*, *104*(3), 87-96.

Taylor, S. R., & McLennan, S. M. (1985). *The continental crust: Its composition and evolution*. Blackwell Scientific.

Yohe, G. (2024). Lithologic Relationship and Structural Features of Crystalline Rocks in Ekiti, Southwestern Nigeria: A Geological Report on the Basement Complex. *Advances in Earth and Environmental Science*, *5*(2), 1-15.

Declaration

Consent for publication

Not Applicable

Availability of data and materials

The publisher has the right to make the data public

Conflict of Interest

The authors declared no conflict of interest

Ethical Considerations

Not applicable

Competing interest

The authors report no conflict or competing interest

Funding

The author declared no source of funding

Authors' Contributions

First Author: Project conceptualization, design, and supervision. Second Author: Writing, results extraction. Third Authur: Analysis, manuscript first draft. Fourth and Fifth Authors: Manuscript revision, review, and proofreading.